NeuroImage 99 (2014) 226–236

Contents lists available at ScienceDirect

NeuroImage

journal homepage: www.elsevier.com/locate/ynimg

Abnormal metabolic connectivity in the pilocarpine-induced epilepsy rat model: A multiscale network analysis based on persistent homology

Hongyoon Choi [a,b], Yu Kyeong Kim [a,c], Hyejin Kang [a], Hyekyoung Lee [a], Hyung-Jun Im [a,b], Do Won Hwang [a,d], E. Edmund Kim [a,b], June-Key Chung [a], Dong Soo Lee [a,b,*]

[a] Department of Nuclear Medicine, Seoul National University College of Medicine, Seoul, Republic of Korea
[b] Department of Molecular Medicine and Biopharmaceutical Sciences, Graduate School of Convergence Science and Technology, Seoul National University, Seoul, Republic of Korea
[c] Department of Nuclear Medicine, Seoul National University Boramae Medical Center, Seoul, Republic of Korea
[d] Institute of Radiation Medicine, Medical Research Center, Seoul, Republic of Korea

ARTICLE INFO

Article history:
Accepted 13 May 2014
Available online 21 May 2014

Keywords:
Epilepsy
FDG PET
Metabolic connectivity
Graph theory
Persistent homology

ABSTRACT

Temporal lobe epilepsy is associated with dysfunctional brain networks. Here we investigated metabolic connectivity in the pilocarpine-induced epilepsy rat model and applied a new multiscale framework to the analysis of metabolic networks of small-animal brains. [^{18}F]fluorodeoxyglucose PET was acquired in pilocarpine-induced chronic epilepsy rats and controls to yield interregional metabolic correlation by inter-subject manner. When interregional correlation of epilepsy rats and controls was compared directly, the epilepsy rats showed reduced connectivity involving the left amygdala and left entorhinal cortex. When regional graph properties were calculated to characterize abnormal nodes in the epileptic brain network, the epilepsy rats showed reduced nodal and local efficiencies in the left amygdala. Then, a new multiscale framework, persistent brain network homology, was used to examine metabolic connectivity with a threshold-free approach and the difference between two networks was analyzed using single linkage distances (SLDs) of all pairwise nodes. We found a tendency for longer SLDs between the left insula/left amygdala and bilateral cortical/subcortical structures in the epilepsy rats. Persistent brain network homology analysis as well as interregional correlation study implied the abnormal left limbic–paralimbic–neocortical network in the pilocarpine-induced epilepsy rat models. In conclusion, we found a globally disrupted network in the epileptic brain in rats, particularly in the limbic and paralimbic structures by direct comparison, graph properties and multiscale network analysis. These results demonstrate that the multiscale and threshold-free network analysis can be used to find the network abnormality in small-animal brains as a preclinical research.

Introduction

Brain function relies on the brain interconnections and many brain disorders present network abnormalities. One of them, epilepsy is a brain network disorder since the ictal discharge initiates from cortical or subcortical structures and propagates to the other brain regions (Blumenfeld et al., 2004; Spencer, 2002). In the clinical setting, patients with epilepsy generally undergo electroencephalography (EEG) and structural MRI to evaluate the epileptogenic zone. However, the propagation of seizure activities from the seizure foci to the adjacent or remote areas is accompanied by various behavioral and cognitive symptoms. Nevertheless, we have been unable to explain language or other cognitive dysfunction with a confined epileptogenic zone localized by routine diagnostic imaging studies (Braakman et al., 2012; Vlooswijk et al., 2010).

Functional neuroimaging studies such as [^{18}F]fluorodeoxyglucose (FDG) positron emission tomography (PET) or perfusion single photon emission computed tomography (SPECT) have been used to localize epileptogenic zones in epilepsy. Interictal FDG PET or ictal SPECT can provide brain metabolism or perfusion, respectively, which is closely related to interictal or ictal brain activity (la Fougere et al., 2009; Lee et al., 2001, 2005, 2006). Recently, not only the localized functional abnormalities in the epileptic brain, but also the interregional connection abnormalities in brain network studies have been reported. EEG and functional or structural MRI studies as well as PET or SPECT were used to investigate network abnormalities (Bernhardt et al., 2011; Bettus et al., 2009; Liao et al., 2010; Sequeira et al., 2013; Trotta et al., 2013; Voets et al., 2012). These approaches suggested that brain networks were disrupted in the epileptic brain, but the abnormalities were not confined to one region in epilepsy patients.

Functional connectivity is defined by statistical association or dependency between brain regions and it can be interpreted as neural interactivity (Friston et al., 1993; Horwitz, 2003). Functional connectivity can be measured by fMRI, PET, EEG, or MEG. An fMRI-based functional

* Corresponding author at: Department of Nuclear Medicine, Seoul National University Hospital 28 Yongon-Dong, Jongno-Gu, Seoul 110-744, Republic of Korea. Fax: 82 2 2072 7690.
E-mail address: dsl@plaza.snu.ac.kr (D.S. Lee).

http://dx.doi.org/10.1016/j.neuroimage.2014.05.039
1053-8119/

connectivity at rest, one of the most commonly used approaches, reflects neuronal correlates of spontaneous fluctuations in blood-oxygen-level-dependent (BOLD) signals between remote cortical regions (Shmuel and Leopold, 2008). Quantitative metabolic measures using PET can be used for functional connectivity because of coupling between neuronal activity and metabolism (Aubert and Costalat, 2002; Herman et al., 2009; Hertz and Zielke, 2004). While the fMRI-based functional connectivity measures temporal correlation of dynamic changes between brain regions, PET-based metabolic connectivity employed regional variations of metabolic demand in the brain (Hyder et al., 2013), with averaged minutes of temporal scale during resting state (i.e., interictal state in this study) (Horwitz et al., 1988; Kang et al., 2003; Lee et al., 2008; Vogt et al., 2006). Since there is no validation study comparing PET-based connectivity to fMRI-based connectivity, and the two approaches might provide different information due to differences in energy consumption coupling (Di et al., 2012; Wehrl et al., 2013), along with fMRI-based functional connectivity and anatomical connectivity (e.g. diffusion tensor imaging), PET-based metabolic connectivity could have complementary role in understanding brain functional connectivity.

To evaluate the complex brain connectivity, graph theoretic approaches were used to measure global topologic features and regional abnormal brain connectomes (Bullmore and Sporns, 2009). Graph theory allows understanding the network characteristics of brain disorders as a complex system. Most of the graph theoretic analysis, including previous studies for the epileptic networks (Bernhardt et al., 2011; Liao et al., 2010), have used threshold to generate the binary networks because weighted network was difficult to interpret. However, when we construct brain connectomes, binary networks are varied according to the threshold, which results in the different graphs and network properties (Fornito et al., 2013; van Wijk et al., 2010). In this study, we employed persistent brain network homology, a new multiscale framework of mathematical modeling for networks, which was generated from all possible thresholds. And thus, it was free from the task of determining proper threshold (Lee et al., 2012b).

The primary purpose of the study was to find abnormal metabolic connectivity in the epilepsy rat model. To investigate metabolic connectivity using FDG PET, brain networks were constructed for each group of rats by inter-subject manner. In the analysis of human brain images, several subject-specific factors (e.g. age and sex) should have been controlled but we could acquire homogenous group of epileptic brains in rat models. We used pilocarpine-induced epilepsy rat models, a well-established animal model for human medial temporal lobe epilepsy (TLE) with controlled subject-specific factors (Curia et al., 2008). Our approach could find abnormal metabolic connection in the brain of epilepsy rat models to explain various neuropsychiatric symptoms in medial TLE. Furthermore, we also investigated whether the new multiscale network framework could be applied to find abnormal topologic features in small-animal model brains for preclinical studies.

Methods

Pilocarpine-induced epilepsy rat models

Adult male Sprague–Dawley (SD) rats (7 weeks old; Koatech, Seoul, Korea), weighing 180–200 g, were used for epilepsy rat models. They were kept at standard laboratory condition (22–24 °C, 12 hour light and dark cycle) with free access to water and standard feed. All the experimental procedures were approved by the Institutional Animal Care and Use Committee at Seoul National University Hospital (IACUC Number 13-0224).

Pilocarpine-induced epilepsy rat models were used in this study as previously reported (Choi et al., 2014). In brief, rats were pretreated with lithium chloride (127 mg/kg, i.p., Sigma, St. Louis, MO) and methylscopolamine-bromide (1 mg/kg, i.p. Sigma) 24 h and 30 min before pilocarpine administration, respectively. Pilocarpine hydrochloride (30 mg/kg, i.p., Sigma) was injected and repeated doses of pilocarpine hydrochloride (10 mg/kg) were then administered every 30 min until stage 4 seizures developed according to the Racine scale (Racine et al., 1972). The control group received lithium chloride, methylscopolamine-bromide and saline (sham treatment) instead of pilocarpine. Diazepam (10 mg/kg, i.p. Samjin, Seoul, Korea) was injected 60 min after the onset of status epilepticus. Repeated diazepam (5 mg/kg) was injected to terminate status epilepticus. After cessation of status epilepticus, rats received intensive care and treated with supplementary moistened and crushed pellets and given 5 mL i.p. injection of 0.9% saline for hydration.

FDG PET acquisition

PET scans were acquired in chronic epilepsy rats and controls. PET images were acquired at 5 weeks after status epilepticus (range 4–6 weeks) in the model group. In control rats, PET scans were acquired at 5 weeks (range 4–5 weeks) also.

PET scans were performed on a dedicated microPET/CT scanner (eXplore VISTA, GE Healthcare, WI). While in an interictal state, rats were anesthesized 2% isoflurane at 1–1.5 L/min oxygen flow for 5–10 min. Rats received an intravenous bolus injection (0.3–0.5 mL/rat) of [^{18}F]FDG (37 MBq/rat) and each rat was awake for the 35 min period of FDG uptake. Static emission scans started at 45 min, which was optimal time for static FDG PET scan in rodents (Schiffer et al., 2007), after FDG injection under anesthesia. Emission scan data were acquired for 20 min with the energy window 400–700 keV. The images were reconstructed by a 3-dimensional ordered-subsets expectation maximum (OSEM) algorithm with attenuation, random and scatter correction (Liu et al., 2001). The voxel size was 0.3875 × 0.3875 × 0.775 mm.

Image preprocessing and parcellation

We used 26 PET images for the connectivity analysis: 16 PET images from models and 10 images from controls. Individual PET images were spatially normalized to the FDG rat brain template (Schiffer et al., 2006) (PMOD 3.4, PMOD group, Zurich, Switzerland) using Statistical Parametric Mapping (SPM2, University College of London, London, UK). Before preprocessing, all voxels of PET images were scaled by a factor of 10 in each dimension to fit approximately the human brain size. All PET images were spatially normalized using nonlinear registration after linear affine transformation. Normalized images were

Table 1
Volume-of-interests and abbreviation.

Region name	Abbreviation
Motor cortex	Mot
Medial prefrontal cortex	MedF
Orbitofrontal cortex	OrbF
Insula	Ins
Parietal association cortex	ParA
Retrosplenial cortex	RSpl
Somatosensory cortex	SS
Cingulate cortex	Cing
Auditory cortex	Aud
Entorhinal cortex	Ento
Hippocampus-anterodorsal	HpA
Hippocampus-posterior	HpP
Amygdala	Amy
Visual cortex	Vis
Nucleus accumbes core/shell	Acb
Caudate–putamen	CP
Thalamus	Tha
Cerebellum	CB

smoothened by Gaussian filter of 12 mm full width at half maximum. The images were segmented into 36 anatomical volume-of-interests (VOIs) (Table 1 with abbreviation of each VOI). We used VOI templates predefined by PMOD software, which was constructed on a 3D digital map based on Paxinos and Watson atlas (Toga et al., 1995). Among the VOIs, we chose cortical, subcortical structures and cerebellum. The value of FDG uptake was globally normalized to the individual gray matter count using SPM2.

Functional connectivity and brain network construction

The method for brain network construction and network analysis procedures are summarized in Fig. 1. To generate brain network, nodes were represented by the VOIs. We acquired intensity-normalized FDG uptake in the VOIs of each subject and correlation coefficients were obtained. Pearson's correlation coefficients (r) between each pair of the VOIs were calculated in an inter-subject manner and correlation matrix (36×36) was obtained for each group, epilepsy rats and controls. A weighted undirected network matrix was constructed for epilepsy rats and controls, where strength of each connection was simply defined as correlation coefficients. We also generated distance matrix, where the distance (c_X) between the nodes was defined as $c_X = 1 - r$. This approach has been previously used to define a metric between nodes in the brain network as a distance of vectors in topological spaces. It can simply change similarity measures between nodes (i.e. correlation coefficients) to dissimilarity ones (Haxby et al., 2001; Kriegeskorte et al., 2008).

Direct connectivity comparison: epilepsy rats vs. controls

To find statistical differences of connectivity between the epilepsy rats and controls, we performed permutation test on all possible connections. Correlation matrix for models and controls were transformed to Z scores using Fisher transformation. Randomly reassigned labels (i.e. models or controls) were permuted 10,000 times for each of 36 VOIs and interregional correlation matrices were calculated, followed by Fisher transformation. We obtained Type I error by the comparison between the observed Z score for each connection and Z score from permuted data. To define statistically different connections, false-discovery-rate (FDR) was used to correct for multiple comparisons at a threshold of $q < 0.05$.

Graph theory analysis

Graph theoretic measurements were used to compare the networks. For each group, we measured the graph theory parameters using only positive links (Kaiser, 2011), where weighted undirected networks were obtained using correlation coefficient matrix. In this study, regional network properties including nodal efficiency (E_{nodal}) and local efficiency (E_{local}) were evaluated for each node (Achard and Bullmore, 2007; Latora and Marchiori, 2001). E_{nodal} and E_{local} allow us to evaluate regional topologic properties without specific threshold. For N nodes and K edges in a graph (G), E_{nodal} for node i is measured as:

$$E_{\text{nodal}}(i) = \frac{1}{N-1} \sum_{i \neq j \in G} \frac{1}{L_{i,j}}$$

where $L_{i,j}$ is the minimum path length between nodes i and j. By definition, E_{nodal} is an inverse of the harmonic mean of the minimum path length between a given node and other nodes in the network. Thus E_{nodal} is closely related to the shortest path length of each node. E_{local} represents the global efficiency (E_{global}) of subgraphs of the neighbors of a given node. E_{global} is the harmonic mean of the minimum path length between all possible pairs of nodes in the network. Because the given node is not an element of subgraphs when E_{local} is estimated, it can reflect the fault tolerance of the network, which means how each of

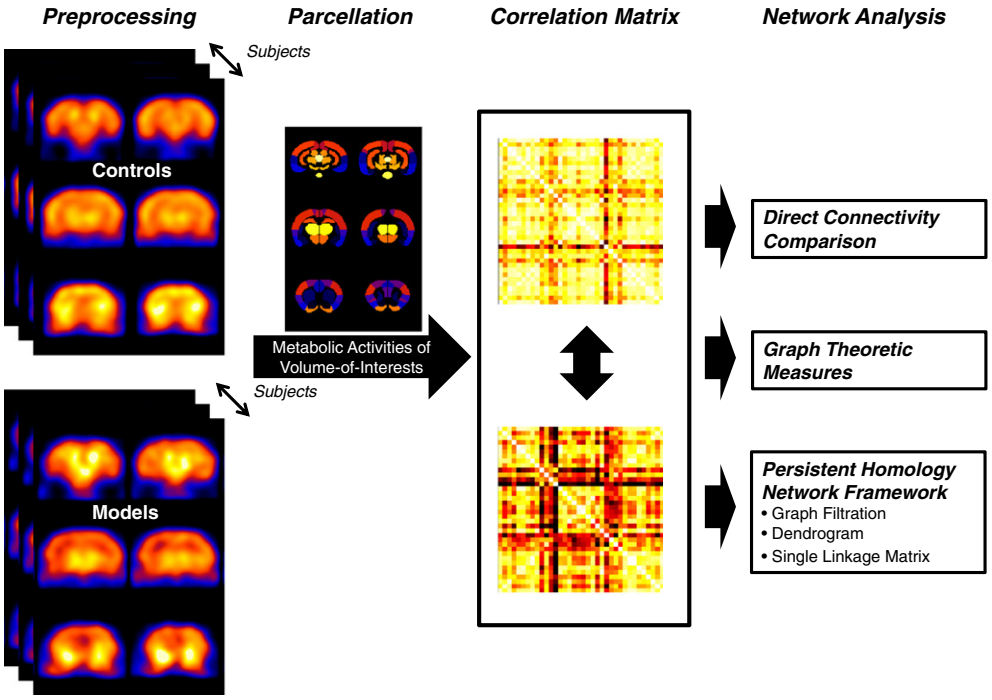

Fig. 1. Flowchart of metabolic connectivity analysis. Firstly, we processed FDG PET images to be spatially normalized. Metabolic activities of each node were obtained by predefined volume-of-interests and interregional correlation coefficient was calculated. All possible connected links in the epilepsy rats and controls were compared. We employed multiscale, threshold-free network modeling framework, persistent homology, to find abnormal metabolic connectivity.

subgraphs containing proper network information when the given node is eliminated. In short, E_{global} and E_{local} are measured as:

$$E_{global}(G) = \frac{1}{N(N-1)} \sum_{i \neq j \in G} \frac{1}{L_{i,j}}$$
$$E_{local}(G_i) = \frac{1}{N_G(N_G-1)} \sum_{j,k \in G} \frac{1}{L_{j,k}}$$

where N_G is the number of nodes in the subgraph G_i.

For global network properties, we employed E_{global} and the characteristic path length ($L_{network}$). $L_{network}$ is the average shortest path length for each node.

$$L_{network}(G) = \frac{1}{N} \sum_{i \in G} \frac{\sum_{i \neq j \in G} L_{i,j}}{N-1}$$

To find statistical difference, we used permutation test for global network parameters including E_{global} and $L_{network}$ as well as for local network parameters, E_{nodal} and E_{local}. The observed regional and global network properties were compared with the network properties iteratively calculated from 10,000 times of randomly reassigned groups and we obtained p-value. To calculate graph theoretic measures, we used Brain Connectivity Toolbox (https://sites.google.com/site/bctnet/).

Multiscale network analysis based on persistent homology

We used multiscale and threshold-free network modeling based on persistent homology to compare the networks of models and controls effectively. Detailed procedures to quantify topological features based on persistent homology were described in a previous study (Lee et al., 2012b). In brief, we used networks generated at every possible threshold and to simplify the computation burden, graph filtration techniques were employed.

Firstly, we generated a sequence of networks as we changed the threshold of distance (ε). When ε increased, topological features of binary networks were changed. As a topological view of brain network, Rips complex was used to represent simplicial complexes. Rips complex is defined as a simplicial complex consisting of nodes and edge, whose k-simplices correspond to edges of a $(k+1)$-simplices which are links of two nodes within distance ε. Rips filtration reflects the multiscale networks, the sequence of the nested Rips complexes over different scales. One of the topological features, Betti number β_0, is a measure of the number of the connected components in the network. We could visualize those topological changes using barcode and dendrogram according to β_0. As ε increases, nodes are connected and using dendrograms, we visually identified how components are merged during Rips filtration.

Single linkage distance (SLD) between the nodes was calculated, which is usually used in hierarchical clustering. Given the network with distance c_X, we calculated SLD (d_X), which was defined as:

$$d_X(x_i, x_j) = \min\left[\max_{l=0,\ldots,k-1} c_X(w_l, w_{l+1}) | x_i = w_0, \ldots, w_k = x_j\right]$$

SLD is the minimum distance between two nodes when they belong to the same connected component during graph filtration. It represents the hierarchical clustered structure of brain network in an algebraic form which can be used for a quantitative measure to discriminate brain networks. Using SLD calculated from persistent network homology, we could obtain the distance between two specific nodes after network construction without specific threshold.

SLD was employed to find different connections between the epilepsy rats and controls. We constructed single linkage matrices (SLM), SLDs between all pairs of nodes. SLMs were constructed with randomly reassigned labels (i.e. models or controls) being permuted 10,000 times. Type I errors were calculated by the comparison between the observed SLD for each connection and SLD from permuted data. Firstly, we applied FDR correction to find significantly different SLDs in epilepsy. To find a global tendency for different SLDs in the epilepsy rats compared to controls, we additionally used uncorrected $p < 0.05$.

Results

Direct comparison of metabolic connectivity: models versus controls

We constructed correlation matrix for each group and Figs. 2A and B represent the c_X maps. For directly comparing the connectivity between controls and epilepsy models, permutation test was performed. Overall, the connectivity in the epilepsy rats was weaker than that in the controls (Figs. 2A–C). Epilepsy rats showed significantly longer c_X between the following pairwise VOIs: left amygdala–left somatosensory cortex, left amygdala–left caudate/putamen, left amygdala–both nucleus accumbens, left entorhinal cortex–left thalamus, left entorhinal cortex–right nucleus accumbens, and right posterior hippocampus–right nucleus accumbens ($q < 0.05$, FDR correction) (Fig. 2D).

Characteristic regional and global graph theory measures in epilepsy rats

A trend toward globally lower E_{nodal} and E_{local}, local network parameters, was found in the epilepsy rats compared to the controls, which were observed in almost all the nodes. Among the differences of the nodes between epilepsy rats from controls, the difference in E_{nodal} and E_{local} of the left amygdala was the highest ($p = 0.017$ for E_{nodal} and $p = 0.007$ for E_{local}) (Figs. 3A and B). The differences of regional graph measures are shown according to their anatomical localization and summarized in Figs. 3C and D.

Globally lower E_{nodal} and E_{local} in the epilepsy rats imply globally inefficient connections between nodes. These differences between epilepsy rats and controls were also found in the global network parameters, E_{global} and $L_{network}$. In the permutation tests, we found significantly lower E_{global} and higher $L_{network}$ in epilepsy rats than those in controls ($p = 0.038$ for E_{global} and $p = 0.047$ for $L_{network}$) (Fig. 4). These differences of the regional and global network properties were considered to represent the disruption of network integrities, thus, the network properties of epilepsy rats more random network topology than those of controls.

Persistent brain network homology revealed dysfunctional left limbic–paralimbic–neocortical network in epilepsy rats

As a threshold-free and multiscale network framework based on persistent homology provides evolutionary changes during the threshold increase, we compared brain networks of epilepsy rats and models in terms of how brain regions (nodes) are connected and clustered during graph filtration.

To visualize network changes during graph filtration upon multiscale brain networks, representative graphs were displayed at different filtration thresholds $\varepsilon = 0.05, 0.10, \ldots, 0.35$ in Fig. 5. Clustering of the brain connections was slower in the epilepsy rats than in controls while ε was increased. The SLD for the each group was computed and converted to the dendrogram displays in Fig. 6. When ε increased, dendrogram (Figs. 6A and B) revealed that clustering occurred later in the hippocampus, amygdala and entorhinal cortex, which belong to the limbic and paralimbic systems, than the other nodes in both the epilepsy and control groups. In epilepsy rats, the clustering was more delayed than in controls. For each connected component, the models showed globally increased SLD compared to controls. This was shown again in single linkage matrix form (Figs. 6C and D).

Epilepsy rats showed a tendency for longer SLDs between some pairwise nodes which could be detected in the permutation tests. When multiple comparison correction (FDR < 0.05) was applied to find significantly different SLDs in the epilepsy rats from controls, there were no edges that survived. When the uncorrected $p < 0.05$ was applied,

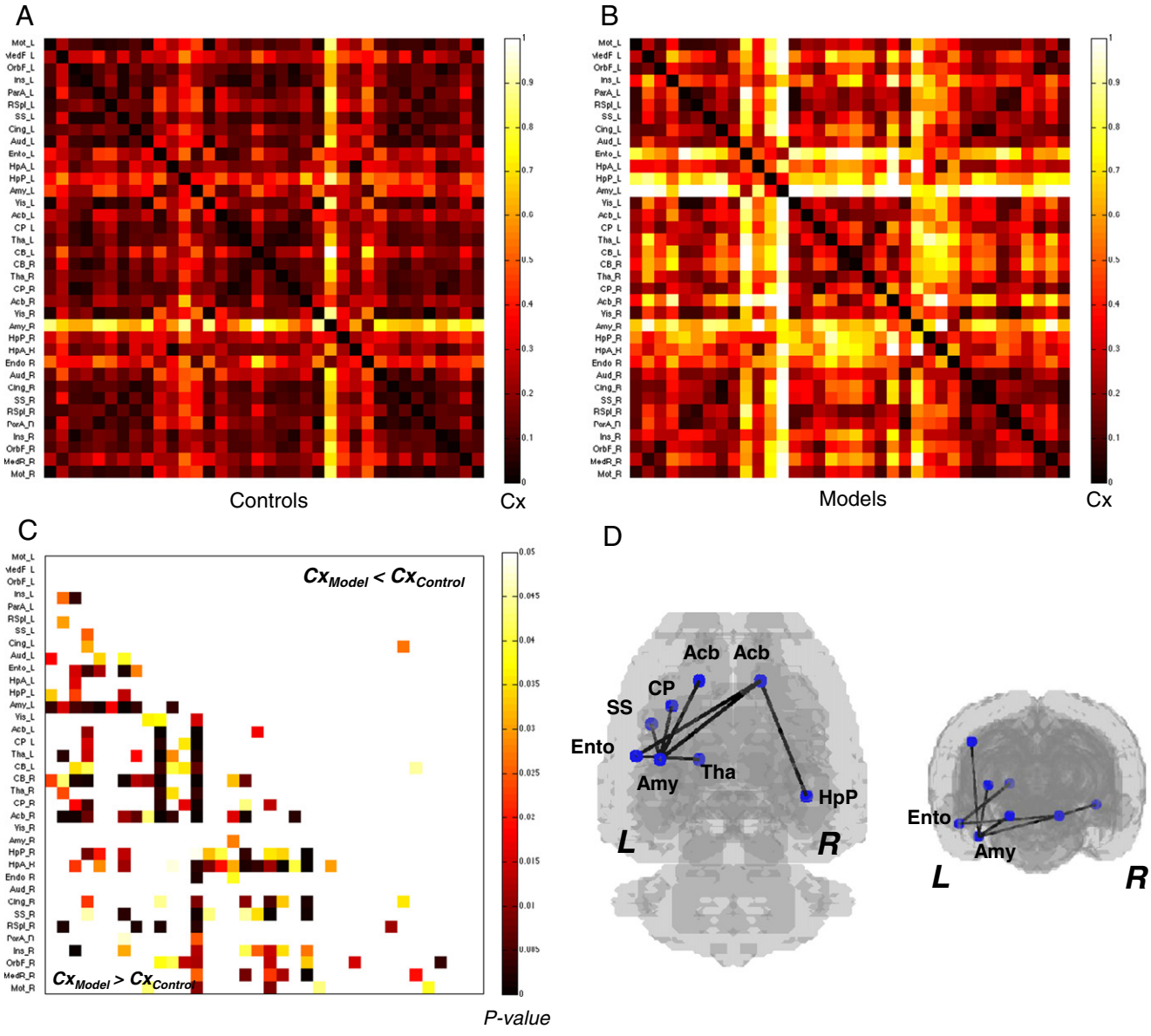

Fig. 2. Metabolic connectivity in the controls and epilepsy rats. (A–B) Distance maps for controls and epilepsy models, respectively. Distances (c_X) between two nodes (i, j) were determined by correlation coefficient (r), simply defined as $c_X(i, j) = 1 - r(i, j)$. (C) To find statistically significant differences in metabolic connectivity between models and controls, we calculated p-values for all possible connections using permutation test. Statistical significance of increased metabolic connectivity (shorter distance) in the epilepsy rats is represented by upper triangular matrix and decreased metabolic connectivity (longer distance) in the epilepsy rats is represented by lower triangular matrix. (D) The anatomical distribution of significantly different links between epilepsy models and controls. In the epilepsy rats, significantly reduced connectivity was found in several pairwise nodes involving the left amygdala and left entorhinal cortex ($q < 0.05$, FDR correction for multiple comparisons).

to find the tendency for different connections in the epilepsy rats, multiple pairwise nodes (edges) showed longer SLDs, mainly involving the connections between the left insular cortex/amygdala and bilateral cortical/subcortical structures (Figs. 7A and B).

Discussion

We analyzed the metabolic connectivity in pilocarpine epilepsy rat models. Direct comparison of the interregional correlation showed significantly decreased connectivity in the pairwise VOIs involving the left amygdala and left entorhinal cortex in the epilepsy rats compared to controls. Graph theoretic measures were significantly different in the epilepsy rats compared with controls, which implied globally and regionally disrupted networks in epileptic brain. E_{nodal} and E_{local} were reduced in almost all nodes in the epilepsy rats and the difference in E_{nodal} and E_{local} between epilepsy rats and controls was the highest in the left amygdala. E_{global} in the epilepsy rats was significantly lower and $L_{network}$ in the epilepsy rats was significantly higher than those in controls. Furthermore, we used persistent homology-based network analysis, which provided how networks were constructed and the linkages of nodes were clustered according to the changes of the thresholds. A tendency for weak connections was found between the left insular cortex/amygdala and bilateral cortical/subcortical structures in the epilepsy rats.

Metabolic brain connectivity

In this study, we obtained interregional metabolic correlations to investigate functional connectivity. Metabolic network analyses could take advantage of the sequential coupling of neuronal activity, regional brain metabolism and perfusion. Thus, metabolic connectivity abnormality might be observed earlier than that of cerebral blood flow connections

(i.e. fMRI or water PET) in progressive brain diseases. Previous studies revealed metabolic connectivity was a sensitive and early diagnostic method in degenerative brain disorders such as Alzheimer's dementia (Morbelli et al., 2012; Seo et al., 2013; Toussaint et al., 2012).

Because metabolic activities measured by PET and fMRI signals reflected different physiologic processes, there is a mismatch between functional networks using those different modalities (Di et al., 2012; Wehrl et al., 2013). Biological signals obtained from two modalities are different, which BOLD signals are contributed by micro- and macrovasculatures (Yu et al., 2012), whereas FDG uptake depends on metabolic demands in neural tissues. Although those previous reports (Di et al., 2012; Wehrl et al., 2013) used different methods from our study for constructing networks, functional connectivity based on a variation of metabolic demands in this study is distinct from tiny fluctuations of BOLD signals, thus, it could be closer to neuronal energy-activity information (Hyder et al., 2011, 2013). BOLD signals indirectly reflect the neuronal activities by measuring a combination of hemodynamic parameters including cerebral blood flow and cerebral blood volume. While widely performed network analyses based on small fluctuations of BOLD signals does not account for baseline neuronal activities which could be the major element, metabolic connectivity constructed by PET reflects directly neuronal energy demands, which could be normalized and adjusted accounting for whole brain activities (Hyder et al., 2011, 2013; Smith et al., 2002).

Recently, interregional correlation analysis in the rodent brain was performed several times using different imaging modalities or ex vivo brain sections. Wang et al. used autoradigraphic cerebral perfusion studies to evaluate brain connectivity (Wang et al., 2011, 2012) and Fidalgo et al. analyzed brain metabolic connectivity measured by cytochrome oxidase immunohistochemistry (Fidalgo et al., 2011). To our knowledge, this is the first study that analyzed metabolic connectivity of in vivo rodent brains using microPET data. To examine interregional correlation using PET images or brain sections, inter-subject correlation was employed. Thus, well-controlled rodent models could

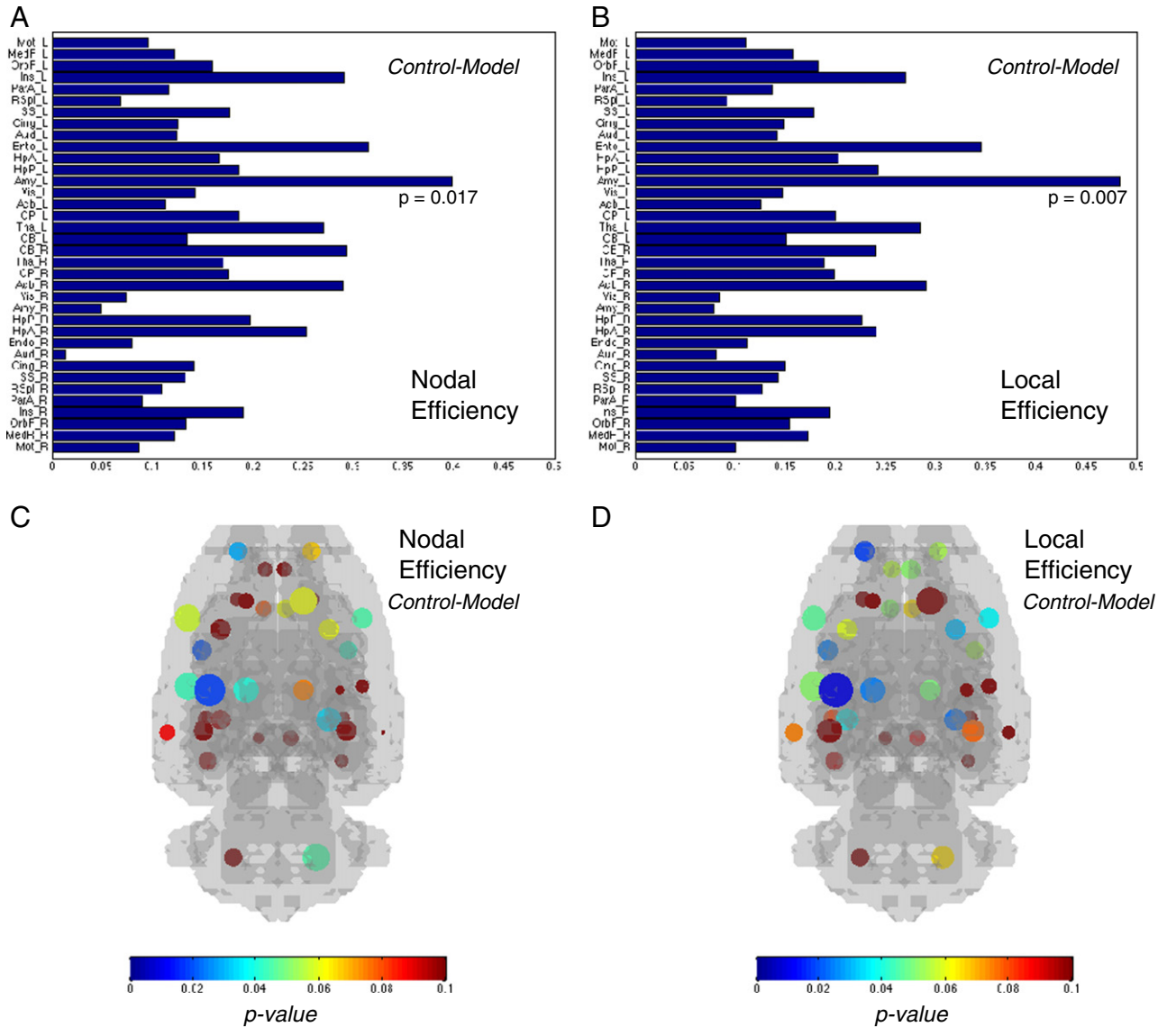

Fig. 3. Difference in regional graph theoretic measures between epilepsy rats and controls. (A) Overall, nodal efficiency E_{nodal} in epilepsy rats was lower than that in controls. The largest difference was found in the left amygdala ($p = 0.017$, uncorrected for multiple comparison). (B) The epilepsy rats showed lower local efficiency E_{local} of each node, particularly in the left amygdala ($p = 0.007$, uncorrected for multiple comparison). (C–D) The nodes are displayed according to their anatomical location. The size of nodes represents difference between two groups and colors of nodes represent statistical significance.

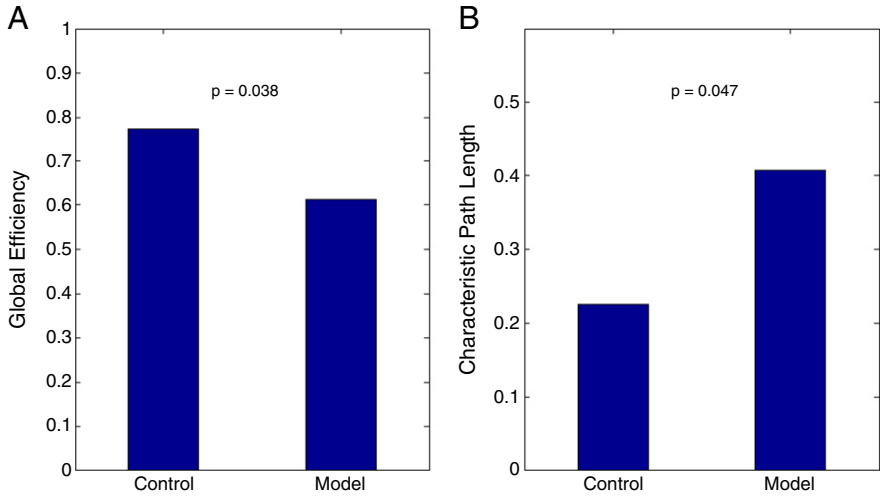

Fig. 4. Global graph theoretic measures. The global network properties, global efficiency E_{global} (A) and characteristic path length $L_{network}$ (B), were displayed. Using permutation test, two parameters were significantly different between epilepsy rats and controls ($p = 0.038$ for global efficiency and $p = 0.047$ for characteristic path length).

have advantages of yielding consistent results with less confounding variables compared to human subject data showing variability of age, gender and other clinical parameters. Various brain disorders including neurodegenerative disease as well as epilepsy can now be evaluated by examining metabolic connectivity in small animals using microPET as a noninvasive imaging tool.

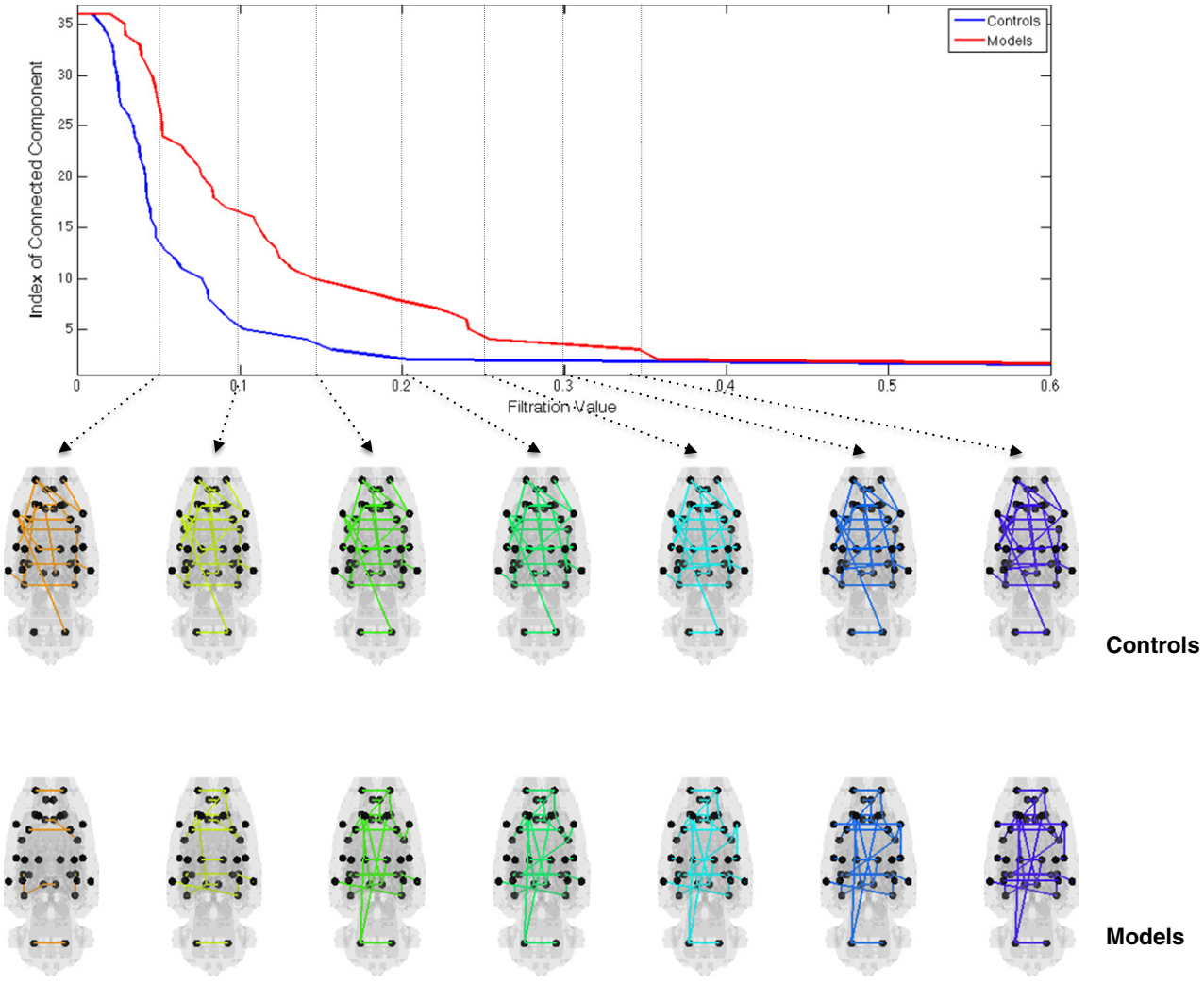

Fig. 5. Graph filtration of epilepsy models and controls. The graphs are shown at seven different filtration values, $\varepsilon = 0.05, 0.10, \ldots, 0.35$. Note that nodes in epilepsy rats were clustered to a giant single component with larger filtration values (distances) than in controls, suggesting globally disrupted and weak connections in epilepsy models.

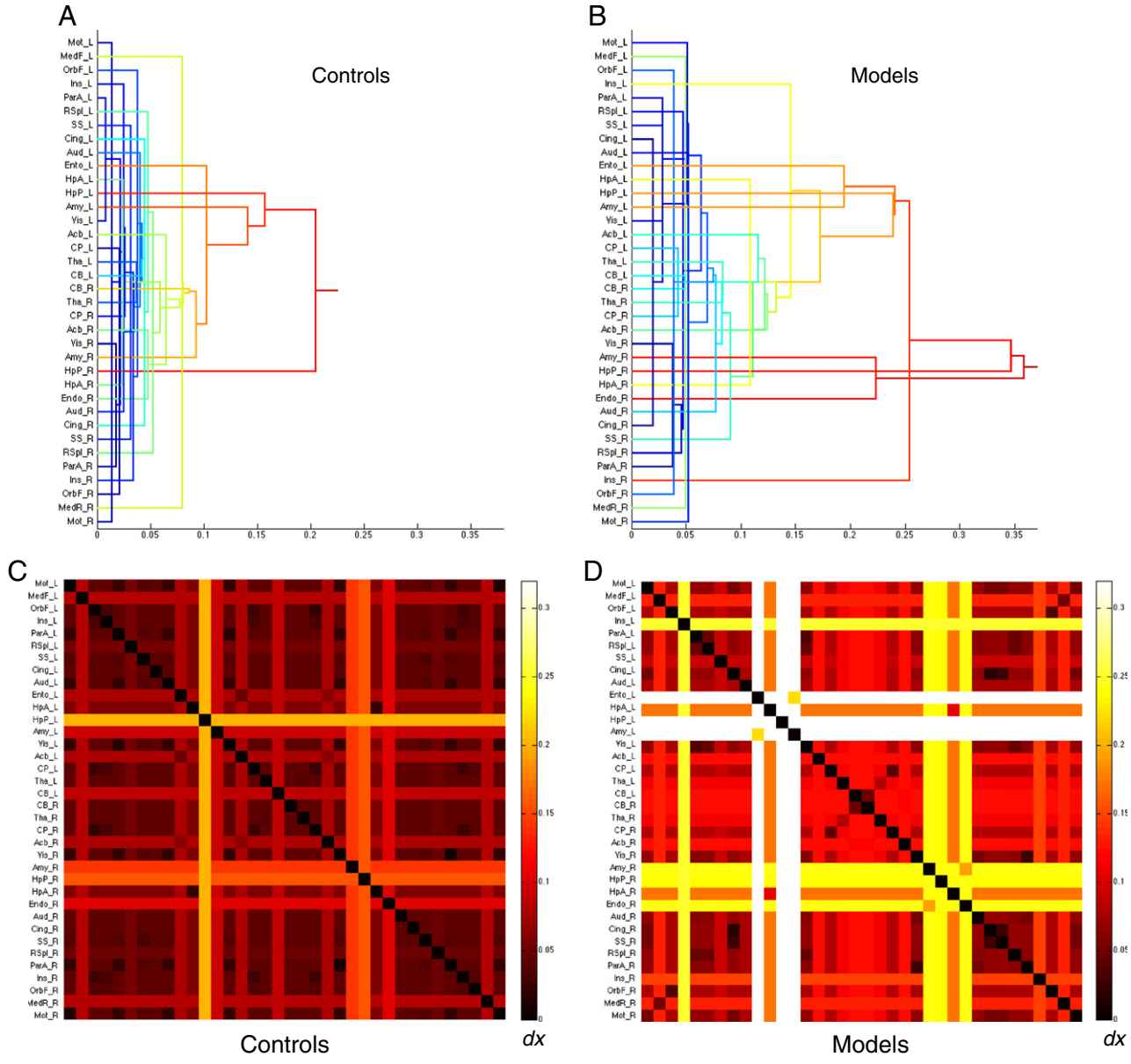

Fig. 6. Single linkage dendrograms and single linkage matrices (SLM) for controls and models. (A–B) Dendrograms represent the evolutionary changes in linked nodes during graph filtration and distance to be merged into the giant component for each connected component. Limbic system showed delayed connections, particularly in the epilepsy rats. (C–D) SLMs calculated from the distance between the paired nodes in controls (C) and models (D). SLMs represented linkages from all possible thresholds and single linkage distances between all possible connections. Dendrograms show which components are merged during Rips filtration and SLMs reveal the recomputed distance between nodes according to the merging.

Abnormal brain connections in the epileptic brain

We found significantly weaker connections, particularly involving the left amygdala and left entorhinal cortex in the epilepsy rats. Furthermore, differences in regional graph properties (i.e. decreased nodal and local efficiencies) were the highest in the left amygdala, followed by left entorhinal cortex. Of note, these brain structures are important in the pilocarpine-induced epilepsy rat model because histopathologic abnormalities such as injured and degenerating neurons were found in these areas as well as in bilateral hippocampi (Mello and Covolan, 1996; Scholl et al., 2013; Turski et al., 1983; Wozny et al., 2005). Pilocarpine-induced epilepsy showed widespread neuronal damage and involved several brain regions (Curia et al., 2008; Scholl et al., 2013), which corresponded to the global network disruption found in this study. Moreover, we found the asymmetric brain network disruption in the epileptic rat brain. To be specific, regional graph theoretic measures were abnormal and connectivity was reduced asymmetrically in the left amygdala and entorhinal cortex in our study, in line with the previous reports. Consistent with the previous EEG data and behavioral features, epileptic discharges were more likely to have initiated in the left hemisphere than in the right hemisphere in the medial TLE patients (Herzog, 1993; Holmes et al., 2001) as well as in the pilocarpine-induced epilepsy rat model (Xia et al., 2009).

Disrupted network integrity in the epilepsy rats reminded the previous fMRI data from human medial TLE patients (Vlooswijk et al., 2011). The differences in regional graph theoretic measures in the epileptic rat brain implied network disruption, closer to random topology than small-world property. Our results coincided with the previous report of network analysis in the rat model, where the authors found the increase in shortest path length and the decrease in clustering coefficient in experimental focal epilepsy models using fMRI (Otte et al., 2012). Electrophysiologic data acquired from the rats with glutamate-injured

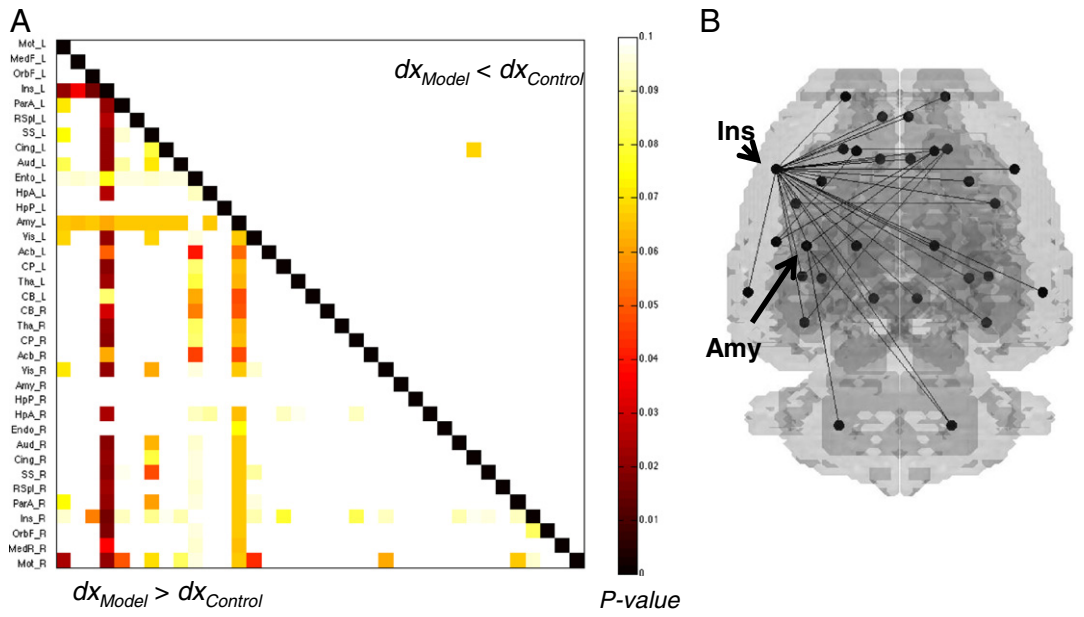

Fig. 7. Group differences in single linkage matrices. (A) We calculated p-values for differences in single linkage distance between all connections using permutation test. Statistical significance of shorter distance in the epilepsy rats is represented by upper triangular matrix and longer distance in the epilepsy rats is represented by lower triangular matrix. (B) Using uncorrected $p < 0.05$ as a threshold, several connections with increased distance in the epilepsy rats were found. A tendency for increased single linkage distances in the epilepsy models was found in several connections, which mainly included the left insular cortex and left amygdala.

hippocampal neuronal network showed also the disruption of small-worldness properties (Srinivas et al., 2007). In spite of different modalities and animal models, disruption in the network properties in epileptic rat brain has been consistently reported.

The abnormal graph theoretic measures characterized by reduced efficiency have been reported in neurodegenerative disorders such as Alzheimer's dementia (Brown et al., 2011; Lo et al., 2010; Seo et al., 2013; Zhao et al., 2012). In chronic medial TLE patients, cognitive impairment is very common and important for neuropsychiatric morbidity (Helmstaedter et al., 2003; Oyegbile et al., 2004). Thus, our finding of disrupted network properties in epilepsy rat models similar to neurodegenerative disorders might be related with the global cognitive changes in epilepsy, though the graph theoretic measures are not the hallmarks of brain dysfunction for cognitive impairment. The global network disruption in the epileptic rat brain can be used to explain various neuropsychiatric features, while regional abnormality in brain perfusion or metabolism cannot explain the diverse cognitive symptoms in chronic medial TLE patients, indicating that medial TLE should be considered as a brain network disorder.

Regional metabolic abnormalities in epilepsy

FDG PET in medial TLE patient is a routine workup procedure in the clinical setting. The patients show hypometabolism in the mesial temporal lobe, which used to extend to the lateral temporal structure (Kim et al., 2003). Previously, Goffin et al. revealed that FDG PET in the chronic pilocarpine epilepsy rat model showed hypometabolism in the left striatum and left entorhinal cortex and hypermetabolism in the brainstem and cerebellum (Goffin et al., 2009). There were different results, as Lee et al. reported that chronic pilocarpine-induced epilepsy model showed hypometabolism in the entire hippocampi and bilateral amygdala (Lee et al., 2012a) while they compared chronic period of epilepsy and baseline. In our results, epilepsy rats showed significant hypometabolism in the cerebral cortex involving anterior cingulate gyrus, bilateral motor cortex, left somatosensory cortex, bilateral anterior hippocampus and left entorhinal cortex (Supplementary Figs. 1 and 2), using voxel-based *T*-test with FDR correction ($p < 0.05$, FDR corrected) compared with sham-treated controls. A small region in the medulla oblongata showed significant hypermetabolism in the epilepsy model, which was much similar to Goffin's previous result. Hypometabolic regions were not limited to the limbic system but involved the cerebral cortex, which might be related to the global network abnormality. We found significantly reduced connectivity across cerebral cortical structures as well as limbic systems, suggesting network disruption between the limbic system and cortex. We think that this could play a role in yielding cortical hypometabolism. In a kainate-induced chronic epilepsy model, similar to the pilocarpine-induced epilepsy model, hypometabolism was reported in the cerebral cortex (Jupp et al., 2012).

Interestingly, the abnormal connectivity found in the network analysis in the present study corresponded, in parts, with regional hypometabolic areas. But, we did not find regional hypometabolism in the left amygdala where the most significant difference was found on regional graph theoretical measures. We suggest that regional hypometabolism reflects the network abnormalities but does not reflect them entirely. The combined effect of the regional hypometabolism and the network abnormalities associated with or without regional abnormalities should be considered to explain brain dysfunction. Of course, the disrupted interregional connectivity could also be observed without regional abnormalities detected on voxel-based analysis. Therefore, regional and global network parameters could provide functional network abnormalities which were not detected on voxel-based analysis to find regional abnormalities.

Determination of abnormalities of the brain network measures may be useful in the clinical setting because extratemporal abnormalities are closely related to surgical outcome in medial TLE (Choi et al., 2003; Theodore et al., 1997). The functional network studies might be used to predict patients' prognosis and to provide correlations of brain network dysfunction with clinical features in the future.

Persistent homology framework for network analysis

We applied a new network modeling method using the persistent homology which Lee et al. reported previously in child patients with

autism spectrum disorder and attention-deficit hyperactivity disorder (Lee et al., 2012b). To avoid using arbitrary thresholds to make binary networks, we applied all the possible thresholds to the inter-regional correlation matrices and found that the networks could be summarized by the subsets of the Rips complex. Multiscale networks were produced for each group and visualized by dendrogram. Single linkage matrix was the equivalent representation of single linkage dendrogram. Upon our analysis, single linkage matrix comparison between epilepsy rats and controls showed a tendency for weak connection involving the left insular cortex as well as left amygdala, though the difference did not reach statistical significance after multiple comparison correction. Of note, insular cortex played an important role in medial TLE, which mediated the spreading of epileptic activity and surgical ablation of the insular cortex reduced seizure activities (Dobesberger et al., 2008; Isnard et al., 2000; Nguyen et al., 2009). Pilocarpine-induced status epilepticus caused interneuron loss in insular cortex (Chen et al., 2010) and insular cortex was regarded as a hub in the progression of epileptic discharges in patients with medial TLE (Maccotta et al., 2013). Therefore, not only the left amygdala and entorhinal cortex, but also the insular cortex could have played roles in epileptic network disruption, suggesting a limbic–paralimbic (i.e. insula and entorhinal cortex)–neocortical connection abnormality in the epileptic rat brain.

In short, we successfully found dysfunctional brain networks in the epileptic rat brain. We showed that the most significant connections in the epilepsy rat models involved the left amygdala and left entorhinal cortex. These areas showed significant changes in the epileptic rat group on graph theoretic measures. Furthermore, SLD increased in the connectomes between the left insular cortex/amygdala and cortical/subcortical structures, which implied abnormally connected network in epilepsy rat brain. Our approaches including direct connectivity comparison, graph theoretic measures, and persistent brain homology-based single linkage matrix consistently showed abnormal connections in the left limbic–paralimbic–neocortical network in the epileptic rat brain.

Conclusion

We demonstrated abnormal metabolic connectivity in the pilocarpine-induced epilepsy rat models. Not only the regional graph theoretic properties but also the functional correlation were significantly different between the epilepsy rats and controls, particularly involving the left amygdala and entorhinal cortex. Using threshold-free network modeling, we also revealed abnormal connections involving the left insular cortex as well as left amygdala. Brain network modeling and the topological properties could provide functional connectivity abnormalities in various brain disorders including epilepsy. Furthermore, our results from small-animal models suggest that functional brain network analysis could be applied to the preclinical studies using rat brain models to yield the hallmarks of various human brain disorders.

Supplementary data to this article can be found online at http://dx.doi.org/10.1016/j.neuroimage.2014.05.039.

Acknowledgments

This work was supported by the future based technology development program of the National Research Foundation (NRF) funded by the MEST (20100028755, NRF-2013R1A2A1A05006227), and MSIP (NRF-2011-0030815) and Basic Science Research Program through the National Research Foundation of Korea (NRF) funded by the Ministry of Education, Science and Technology (2012R1A1A2008799), and a grant of the Korean Health Technology R&D Project, Ministry of Health & Welfare, Republic of Korea (HI13C1299).

Disclosures

None declared.

References

Achard, S., Bullmore, E., 2007. Efficiency and cost of economical brain functional networks. PLoS Comput. Biol. 3, e17.
Aubert, A., Costalat, R., 2002. A model of the coupling between brain electrical activity, metabolism, and hemodynamics: application to the interpretation of functional neuroimaging. NeuroImage 17, 1162–1181.
Bernhardt, B.C., Chen, Z., He, Y., Evans, A.C., Bernasconi, N., 2011. Graph-theoretical analysis reveals disrupted small-world organization of cortical thickness correlation networks in temporal lobe epilepsy. Cereb. Cortex 21, 2147–2157.
Bettus, G., Guedj, E., Joyeux, F., Confort-Gouny, S., Soulier, E., Laguitton, V., Cozzone, P.J., Chauvel, P., Ranjeva, J.P., Bartolomei, F., Guye, M., 2009. Decreased basal fMRI functional connectivity in epileptogenic networks and contralateral compensatory mechanisms. Hum. Brain Mapp. 30, 1580–1591.
Blumenfeld, H., McNally, K.A., Vanderhill, S.D., Paige, A.L., Chung, R., Davis, K., Norden, A.D., Stokking, R., Studholme, C., Novotny Jr., E.J., Zubal, I.G., Spencer, S.S., 2004. Positive and negative network correlations in temporal lobe epilepsy. Cereb. Cortex 14, 892–902.
Braakman, H.M., van der Kruijs, S.J., Vaessen, M.J., Jansen, J.F., Debeij-van Hall, M.H., Vles, J. S., Aldenkamp, A.P., Backes, W.H., Hofman, P.A., 2012. Microstructural and functional MRI studies of cognitive impairment in epilepsy. Epilepsia 53, 1690–1699.
Brown, J.A., Terashima, K.H., Burggren, A.C., Ercoli, L.M., Miller, K.J., Small, G.W., Bookheimer, S.Y., 2011. Brain network local interconnectivity loss in aging APOE-4 allele carriers. Proc. Natl. Acad. Sci. U. S. A. 108, 20760–20765.
Bullmore, E., Sporns, O., 2009. Complex brain networks: graph theoretical analysis of structural and functional systems. Nat. Rev. Neurosci. 10, 186–198.
Chen, S., Fujita, S., Koshikawa, N., Kobayashi, M., 2010. Pilocarpine-induced status epilepticus causes acute interneuron loss and hyper-excitatory propagation in rat insular cortex. Neuroscience 166, 341–353.
Choi, J.Y., Kim, S.J., Hong, S.B., Seo, D.W., Hong, S.C., Kim, B.T., Kim, S.E., 2003. Extratemporal hypometabolism on FDG PET in temporal lobe epilepsy as a predictor of seizure outcome after temporal lobectomy. Eur. J. Nucl. Med. Mol. Imaging 30, 581–587.
Choi, H., Kim, Y.K., Oh, S.W., Im, H.J., Kang, H., Lee, B., Lee, Y.S., Jeong, J.M., Kim, E.E., Chung, J.K., Lee, D.S., 2014. In vivo imaging of mGluR5 changes during epileptogenesis using [^{11}C] ABP688 PET in pilocarpine-induced epilepsy rat model. PLoS One 9, e92765.
Curia, G., Longo, D., Biagini, G., Jones, R.S., Avoli, M., 2008. The pilocarpine model of temporal lobe epilepsy. J. Neurosci. Methods 172, 143–157.
Di, X., Biswal, B.B., Alzheimer's Disease Neuroimaging, I., 2012. Metabolic brain covariant networks as revealed by FDG-PET with reference to resting-state fMRI networks. Brain Connect. 2, 275–283.
Dobesberger, J., Ortler, M., Unterberger, I., Walser, G., Falkenstetter, T., Bodner, T., Benke, T., Bale, R., Fiegele, T., Donnemiller, E., Gotwald, T., Trinka, E., 2008. Successful surgical treatment of insular epilepsy with nocturnal hypermotor seizures. Epilepsia 49, 159–162.
Fidalgo, C., Conejo, N.M., Gonzalez-Pardo, H., Arias, J.L., 2011. Cortico-limbic-striatal contribution after response and reversal learning: a metabolic mapping study. Brain Res. 1368, 143–150.
Fornito, A., Zalesky, A., Breakspear, M., 2013. Graph analysis of the human connectome: promise, progress, and pitfalls. NeuroImage 80, 426–444.
Friston, K.J., Frith, C.D., Liddle, P.F., Frackowiak, R.S., 1993. Functional connectivity: the principal-component analysis of large (PET) data sets. J. Cereb. Blood Flow Metab. 13, 5–14.
Goffin, K., Van Paesschen, W., Dupont, P., Van Laere, K., 2009. Longitudinal microPET imaging of brain glucose metabolism in rat lithium–pilocarpine model of epilepsy. Exp. Neurol. 217, 205–209.
Haxby, J.V., Gobbini, M.I., Furey, M.L., Ishai, A., Schouten, J.L., Pietrini, P., 2001. Distributed and overlapping representations of faces and objects in ventral temporal cortex. Science 293, 2425–2430.
Helmstaedter, C., Kurthen, M., Lux, S., Reuber, M., Elger, C.E., 2003. Chronic epilepsy and cognition: a longitudinal study in temporal lobe epilepsy. Ann. Neurol. 54, 425–432.
Herman, P., Sanganahalli, B.G., Blumenfeld, H., Hyder, F., 2009. Cerebral oxygen demand for short-lived and steady-state events. J. Neurochem. 109 (Suppl. 1), 73–79.
Hertz, L., Zielke, H.R., 2004. Astrocytic control of glutamatergic activity: astrocytes as stars of the show. Trends Neurosci. 27, 735–743.
Herzog, A.G., 1993. A relationship between particular reproductive endocrine disorders and the laterality of epileptiform discharges in women with epilepsy. Neurology 43, 1907–1910.
Holmes, M.D., Dodrill, C.B., Kutsy, R.L., Ojemann, G.A., Miller, J.W., 2001. Is the left cerebral hemisphere more prone to epileptogenesis than the right? Epileptic Disord. 3, 137–141.
Horwitz, B., 2003. The elusive concept of brain connectivity. NeuroImage 19, 466–470.
Horwitz, B., Rumsey, J.M., Grady, C.L., Rapoport, S.I., 1988. The cerebral metabolic landscape in autism. Intercorrelations of regional glucose utilization. Arch. Neurol. 45, 749–755.
Hyder, F., Herman, P., Sanganahalli, B.G., Coman, D., Blumenfeld, H., Rothman, D.L., 2011. Role of ongoing, intrinsic activity of neuronal populations for quantitative neuroimaging of functional magnetic resonance imaging-based networks. Brain Connect. 1, 185–193.
Hyder, F., Fulbright, R.K., Shulman, R.G., Rothman, D.L., 2013. Glutamatergic function in the resting awake human brain is supported by uniformly high oxidative energy. J. Cereb. Blood Flow Metab. 33, 339–347.

Isnard, J., Guenot, M., Ostrowsky, K., Sindou, M., Mauguiere, F., 2000. The role of the insular cortex in temporal lobe epilepsy. Ann. Neurol. 48, 614–623.
Jupp, B., Williams, J., Binns, D., Hicks, R.J., Cardamone, L., Jones, N., Rees, S., O'Brien, T.J., 2012. Hypometabolism precedes limbic atrophy and spontaneous recurrent seizures in a rat model of TLE. Epilepsia 53, 1233–1244.
Kaiser, M., 2011. A tutorial in connectome analysis: topological and spatial features of brain networks. NeuroImage 57, 892–907.
Kang, E., Lee, D.S., Lee, J.S., Kang, H., Hwang, C.H., Oh, S.H., Kim, C.S., Chung, J.K., Lee, M.C., Jang, M.J., Lee, Y.J., Morosan, P., Zilles, K., 2003. Developmental hemispheric asymmetry of interregional metabolic correlation of the auditory cortex in deaf subjects. NeuroImage 19, 777–783.
Kim, Y.K., Lee, D.S., Lee, S.K., Kim, S.K., Chung, C.K., Chang, K.H., Choi, K.Y., Chung, J.K., Lee, M.C., 2003. Differential features of metabolic abnormalities between medial and lateral temporal lobe epilepsy: quantitative analysis of (18)F-FDG PET using SPM. J. Nucl. Med. 44, 1006–1012.
Kriegeskorte, N., Mur, M., Ruff, D.A., Kiani, R., Bodurka, J., Esteky, H., Tanaka, K., Bandettini, P.A., 2008. Matching categorical object representations in inferior temporal cortex of man and monkey. Neuron 60, 1126–1141.
la Fougere, C., Rominger, A., Forster, S., Geisler, J., Bartenstein, P., 2009. PET and SPECT in epilepsy: a critical review. Epilepsy Behav. 15, 50–55.
Latora, V., Marchiori, M., 2001. Efficient behavior of small-world networks. Phys. Rev. Lett. 87.
Lee, D.S., Lee, S.K., Lee, M.C., 2001. Functional neuroimaging in epilepsy: FDG PET and ictal SPECT. J. Korean Med. Sci. 16, 689–696.
Lee, J.J., Kang, W.J., Lee, D.S., Lee, J.S., Hwang, H., Kim, K.J., Hwang, Y.S., Chung, J.K., Lee, M.C., 2005. Diagnostic performance of 18F-FDG PET and ictal 99mTc-HMPAO SPET in pediatric temporal lobe epilepsy: quantitative analysis by statistical parametric mapping, statistical probabilistic anatomical map, and subtraction ictal SPET. Seizure 14, 213–220.
Lee, S.K., Lee, S.Y., Yun, C.H., Lee, H.Y., Lee, J.S., Lee, D.S., 2006. Ictal SPECT in neocortical epilepsies: clinical usefulness and factors affecting the pattern of hyperperfusion. Neuroradiology 48, 678–684.
Lee, D.S., Kang, H., Kim, H., Park, H., Oh, J.S., Lee, J.S., Lee, M.C., 2008. Metabolic connectivity by interregional correlation analysis using statistical parametric mapping (SPM) and FDG brain PET; methodological development and patterns of metabolic connectivity in adults. Eur. J. Nucl. Med. Mol. Imaging 35, 1681–1691.
Lee, E.M., Park, G.Y., Im, K.C., Kim, S.T., Woo, C.W., Chung, J.H., Kim, K.S., Kim, J.S., Shon, Y. M., Kim, Y.I., Kang, J.K., 2012a. Changes in glucose metabolism and metabolites during the epileptogenic process in the lithium–pilocarpine model of epilepsy. Epilepsia 53, 860–869.
Lee, H., Kang, H., Chung, M.K., Kim, B.N., Lee, D.S., 2012b. Persistent brain network homology from the perspective of dendrogram. IEEE Trans. Med. Imaging 31, 2267–2277.
Liao, W., Zhang, Z., Pan, Z., Mantini, D., Ding, J., Duan, X., Luo, C., Lu, G., Chen, H., 2010. Altered functional connectivity and small-world in mesial temporal lobe epilepsy. PLoS One 5, e8525.
Liu, X., Comtat, C., Michel, C., Kinahan, P., Defrise, M., Townsend, D., 2001. Comparison of 3-D reconstruction with 3D-OSEM and with FORE + OSEM for PET. IEEE Trans. Med. Imaging 20, 804–814.
Lo, C.Y., Wang, P.N., Chou, K.H., Wang, J., He, Y., Lin, C.P., 2010. Diffusion tensor tractography reveals abnormal topological organization in structural cortical networks in Alzheimer's disease. J. Neurosci. 30, 16876–16885.
Maccotta, L., He, B.J., Snyder, A.Z., Eisenman, L.N., Benzinger, T.L., Ances, B.M., Corbetta, M., Hogan, R.E., 2013. Impaired and facilitated functional networks in temporal lobe epilepsy. NeuroImage Clin. 2, 862–872.
Mello, L.E., Covolan, L., 1996. Spontaneous seizures preferentially injure interneurons in the pilocarpine model of chronic spontaneous seizures. Epilepsy Res. 26, 123–129.
Morbelli, S., Drzezga, A., Perneczky, R., Frisoni, G.B., Caroli, A., van Berckel, B.N., Ossenkoppele, R., Guedj, E., Didic, M., Brugnolo, A., Sambuceti, G., Pagani, M., Salmon, E., Nobili, F., 2012. Resting metabolic connectivity in prodromal Alzheimer's disease. A European Alzheimer Disease Consortium (EADC) project. Neurobiol. Aging 33, 2533–2550.
Nguyen, D.K., Nguyen, D.B., Malak, R., Leroux, J.M., Carmant, L., Saint-Hilaire, J.M., Giard, N., Cossette, P., Bouthillier, A., 2009. Revisiting the role of the insula in refractory partial epilepsy. Epilepsia 50, 510–520.
Otte, W.M., Dijkhuizen, R.M., van Meer, M.P., van der Hel, W.S., Verlinde, S.A., van Nieuwenhuizen, O., Viergever, M.A., Stam, C.J., Braun, K.P., 2012. Characterization of functional and structural integrity in experimental focal epilepsy: reduced network efficiency coincides with white matter changes. PLoS One 7, e39078.
Oyegbile, T.O., Dow, C., Jones, J., Bell, B., Rutecki, P., Sheth, R., Seidenberg, M., Hermann, B.P., 2004. The nature and course of neuropsychological morbidity in chronic temporal lobe epilepsy. Neurology 62, 1736–1742.
Racine, R., Okujava, V., Chipashvili, S., 1972. Modification of seizure activity by electrical stimulation. 3. Mechanisms. Electroencephalogr. Clin. Neurophysiol. 32, 295–299.
Schiffer, W.K., Mirrione, M.M., Biegon, A., Alexoff, D.L., Patel, V., Dewey, S.L., 2006. Serial microPET measures of the metabolic reaction to a microdialysis probe implant. J. Neurosci. Methods 155, 272–284.
Schiffer, W.K., Mirrione, M.M., Dewey, S.L., 2007. Optimizing experimental protocols for quantitative behavioral imaging with 18F-FDG in rodents. J. Nucl. Med. 48, 277–287.
Scholl, E.A., Dudek, F.E., Ekstrand, J.J., 2013. Neuronal degeneration is observed in multiple regions outside the hippocampus after lithium pilocarpine-induced status epilepticus in the immature rat. Neuroscience 252, 45–59.
Seo, E.H., Lee, D.Y., Lee, J.M., Park, J.S., Sohn, B.K., Lee, D.S., Choe, Y.M., Woo, J.I., 2013. Whole-brain functional networks in cognitively normal, mild cognitive impairment, and Alzheimer's disease. PLoS One 8, e53922.
Sequeira, K.M., Tabesh, A., Sainju, R.K., DeSantis, S.M., Naselaris, T., Joseph, J.E., Ahlman, M.A., Spicer, K.M., Glazier, S.S., Edwards, J.C., Bonilha, L., 2013. Perfusion network shift during seizures in medial temporal lobe epilepsy. PLoS One 8, e53204.
Shmuel, A., Leopold, D.A., 2008. Neuronal correlates of spontaneous fluctuations in fMRI signals in monkey visual cortex: implications for functional connectivity at rest. Hum. Brain Mapp. 29, 751–761.
Smith, A.J., Blumenfeld, H., Behar, K.L., Rothman, D.L., Shulman, R.G., Hyder, F., 2002. Cerebral energetics and spiking frequency: the neurophysiological basis of fMRI. Proc. Natl. Acad. Sci. U. S. A. 99, 10765–10770.
Spencer, S.S., 2002. Neural networks in human epilepsy: evidence of and implications for treatment. Epilepsia 43, 219–227.
Srinivas, K.V., Jain, R., Saurav, S., Sikdar, S.K., 2007. Small-world network topology of hippocampal neuronal network is lost, in an in vitro glutamate injury model of epilepsy. Eur. J. Neurosci. 25, 3276–3286.
Theodore, W.H., Sato, S., Kufta, C.V., Gaillard, W.D., Kelley, K., 1997. FDG-positron emission tomography and invasive EEG: seizure focus detection and surgical outcome. Epilepsia 38, 81–86.
Toga, A.W., Santori, E.M., Hazani, R., Ambach, K., 1995. A 3D digital map of rat brain. Brain Res. Bull. 38, 77–85.
Toussaint, P.J., Perlbarg, V., Bellec, P., Desarnaud, S., Lacomblez, L., Doyon, J., Habert, M.O., Benali, H., Benali, for the Alzheimer's Disease Neuroimaging Initiative, 2012. Resting state FDG-PET functional connectivity as an early biomarker of Alzheimer's disease using conjoint univariate and independent component analyses. NeuroImage 63, 936–946.
Trotta, N., Goldman, S., Legros, B., Baete, K., Van Laere, K., Van Bogaert, P., De Tiege, X., 2013. Changes in functional integration with the non-epileptic temporal lobe of patients with unilateral mesiotemporal epilepsy. PLoS One 8, e67053.
Turski, W.A., Cavalheiro, E.A., Schwarz, M., Czuczwar, S.J., Kleinrok, Z., Turski, L., 1983. Limbic seizures produced by pilocarpine in rats: behavioural, electroencephalographic and neuropathological study. Behav. Brain Res. 9, 315–335.
van Wijk, B.C., Stam, C.J., Daffertshofer, A., 2010. Comparing brain networks of different size and connectivity density using graph theory. PLoS One 5, e13701.
Vlooswijk, M.C., Jansen, J.F., Majoie, H.J., Hofman, P.A., de Krom, M.C., Aldenkamp, A.P., Backes, W.H., 2010. Functional connectivity and language impairment in cryptogenic localization-related epilepsy. Neurology 75, 395–402.
Vlooswijk, M.C., Vaessen, M.J., Jansen, J.F., de Krom, M.C., Majoie, H.J., Hofman, P.A., Aldenkamp, A.P., Backes, W.H., 2011. Loss of network efficiency associated with cognitive decline in chronic epilepsy. Neurology 77, 938–944.
Voets, N.L., Beckmann, C.F., Cole, D.M., Hong, S., Bernasconi, A., Bernasconi, N., 2012. Structural substrates for resting network disruption in temporal lobe epilepsy. Brain 135, 2350–2357.
Vogt, B.A., Vogt, L., Laureys, S., 2006. Cytology and functionally correlated circuits of human posterior cingulate areas. NeuroImage 29, 452–466.
Wang, Z., Bradesi, S., Charles, J.R., Pang, R.D., Maarek, J.M., Mayer, E.A., Holschneider, D.P., 2011. Functional brain activation during retrieval of visceral pain-conditioned passive avoidance in the rat. Pain 152, 2746–2756.
Wang, Z., Pang, R.D., Hernandez, M., Ocampo, M.A., Holschneider, D.P., 2012. Anxiolytic-like effect of pregabalin on unconditioned fear in the rat: an autoradiographic brain perfusion mapping and functional connectivity study. NeuroImage 59, 4168–4188.
Wehrl, H.F., Hossain, M., Lankes, K., Liu, C.C., Bezrukov, I., Martirosian, P., Schick, F., Reischl, G., Pichler, B.J., 2013. Simultaneous PET-MRI reveals brain function in activated and resting state on metabolic, hemodynamic and multiple temporal scales. Nat. Med. 19, 1184–1189.
Wozny, C., Gabriel, S., Jandova, K., Schulze, K., Heinemann, U., Behr, J., 2005. Entorhinal cortex entrains epileptiform activity in CA1 in pilocarpine-treated rats. Neurobiol. Dis. 19, 451–460.
Xia, Y., Lai, Y., Lei, L., Liu, Y., Yao, D., 2009. Left hemisphere predominance of pilocarpine-induced rat epileptiform discharges. J. Neuroeng. Rehabil. 6, 42.
Yu, X., Glen, D., Wang, S., Dodd, S., Hirano, Y., Saad, Z., Reynolds, R., Silva, A.C., Koretsky, A.P., 2012. Direct imaging of macrovascular and microvascular contributions to BOLD fMRI in layers IV–V of the rat whisker-barrel cortex. NeuroImage 59, 1451–1460.
Zhao, X., Liu, Y., Wang, X., Liu, B., Xi, Q., Guo, Q., Jiang, H., Jiang, T., Wang, P., 2012. Disrupted small-world brain networks in moderate Alzheimer's disease: a resting-state FMRI study. PLoS One 7, e33540.